Inception of ice accretion by ice crystal impact

Jens Löwe[1], Daniel Kintea[1], Arne Baumert[2], Stephan Bansmer[2], Ilia V. Roisman[1,3], Cameron Tropea[1,3]

[1]Institute for Fluid Mechanics and Aerodynamics, Technische Universität Darmstadt, Darmstadt, Germany
[2]Institute for Fluid Mechanics, Technische Universität Braunschweig, Braunschweig, Germany
[3]Center of Smart Interfaces, Technische Universität Darmstadt, Darmstadt, Germany

E-mail: s.bansmer@tu-braunschweig.de

Abstract. In this experimental and theoretical study the ice accretion phenomena on a heated cylinder in Braunschweig Icing Wind Tunnel are investigated. The ice crystal size, velocity, the liquid-to-total mass ratio are accurately controlled. The evolution of the cylinder temperature, the time required for the inception of the ice accretion, and the ice accretion rate are measured for various operating conditions.

The surface temperature of the solid target is determined by balancing the heating power in the wall and the cooling effect of the stream of ice particles. We have discovered that the inception of the ice crystal accretion is determined by the instant when the surface temperature of the heated target reduces to the freezing temperature. This result will help to model the phenomena of ice crystal accretion

1. Introduction

The reliability of aircraft and the safety of the passengers is one of the fundamental concerns of the aviation industry. The International Air Transport Association (IATA) defines the safety of flying as the number one priority [1, 2]. One of the reasons which could lead to technical failures is the icing of aircraft parts. There are several mechanisms which cause icing. One mechanism is related to the presence of supercooled liquid droplets in clouds [3, 4, 5]. Further mechanism of icing is attributed to the impact of ice crystals, which usually occurs at relatively high altitudes, higher than 6700 m, typically in deep convective cloud systems.

Cold surfaces are not influenced by the impingement of ice crystals, because they bounce off the surface. In contrast, warm surfaces, like the stator blades of a low pressure compressor, may be affected by the impinging ice crystals [3]. Inside the engine the temperature is higher than the freezing temperature, which causes the ice crystals to partially melt and deposit on the solid surfaces. Due to the formed ice layer, the cross-section of the flow inside the compressor is reduced and the flow around the stator blades is influenced. Ice crystal accretion can lead to stall, surge and instability of the flow inside the engine [6]. A detached flow inside the turbine induces a power loss of the engine. Moreover, shedding of the adhered ice could then cause damage to other downstream parts of the engine or a flame-out. Sensors can also be affected by ice crystal accretion.

The Federal Aviation Administration (FAA) has recently updated their regulations for the certification of an aircraft and their engines with respect to ice crystal icing [7]. Due to this fact

there is great interest in the aviation industry to improve the knowledge of the ice crystal icing mechanism.

The icing of a non-heated cylinder was investigated by several authors. Launiaien and Lyyra [8] investigated the icing of a cylinder due to water droplets in an air flow and analyzed the shape as well as the size of ice accretion. Also Lozowski and Stallabrass [9] performed experiments to investigate the icing of a non-rotating cylinder [10]. Additionally they developed an ice accretion model by investigating the impact of droplets as well as the heat transfer of the cylinder .

Al-Khalil and Irani [11] performed several experiments, with both water droplets and ice crystals, in the Cox wind tunnel. They investigated the ice growth on an airfoil. More experiments were performed by Mason et. al. [12] who used a generic model of an aircraft engine compressor inlet to investigate the accretion. The ice particles were introduced into the flow with different temperatures and the surface temperature, the accretion position as well as the amount of accretion were investigated. They developed a theory for an optimum icing regime, which depends on the liquid and water content in the air flow.
Further experiments were performed in Struk et al. [13], who investigated the ice accretion on an inclined airfoil. They used a wedge airfoil as a model with different surface materials and investigated the accretion of ice depending on the temperature, the liquid water content and the ice water content. These experiments were extended in [14] by integrating heaters inside the airfoil. The airfoil was heated and they investigated the interaction between the ice accretion and the applied heat flux. In particular, they observed also the shedding phenomena of the ice layer. Depending on the conditions, an ice layer is formed and periodically shed from the surface. The determined growth rates of the ice were almost linear.
Additional experiments were performed in [15], where the icing of a hemisphere was studied as a function of the liquid water content. They determined the shape of the ice accretion and used this information to develop an empirical model for ice growth.

The impact of a single ice particle onto a dry surface leading to its breakup was studied recently in [16, 17]. The threshold velocity for minor and major particle breakup, the duration of the collision and the diameter of the contact area between the particle and the substrate were determined. This study is helpful to model also the thermal effects related to a particle impact onto a solid substrate.

The main subject of the present study is an investigation of the early stages of ice crystal accretion. In particular, the evolution of the substrate temperature before ice accretion is measured in an icing wind tunnel and is modelled theoretically. The conditions and the time required for the accretion inception are determined.

2. Experimental method

The experimental setup in the present study consists of an icing wind tunnel, an ice particle generation system, a data acquisition and control system, an experimental cell (which includes a heated solid cylindrical target), and an optical observation system.

2.1. Icing wind tunnel

All experiments were performed in the Braunschweig icing wind tunnel pictured in Fig. 1. It is a closed-looped system, also known as a Göttinger tunnel. The air is accelerated by a fan, located at the upper part of the wind tunnel, reaching a maximum velocity of 40 m/s in a test section [18]. Behind the fan the airflow enters the heat exchanger. Inside the heat exchanger the air is cooled to the desired temperature, which covers a range from -20 °C to +20 °C [18]. The flow enters a settling chamber and is guided through a nozzle, which leads the air into the closed test section. The test section of the tunnel has a quadratic area with a side length of 0.5 m. For optical access several windows on the sides as well as on the top and the bottom are integrated into the test section.

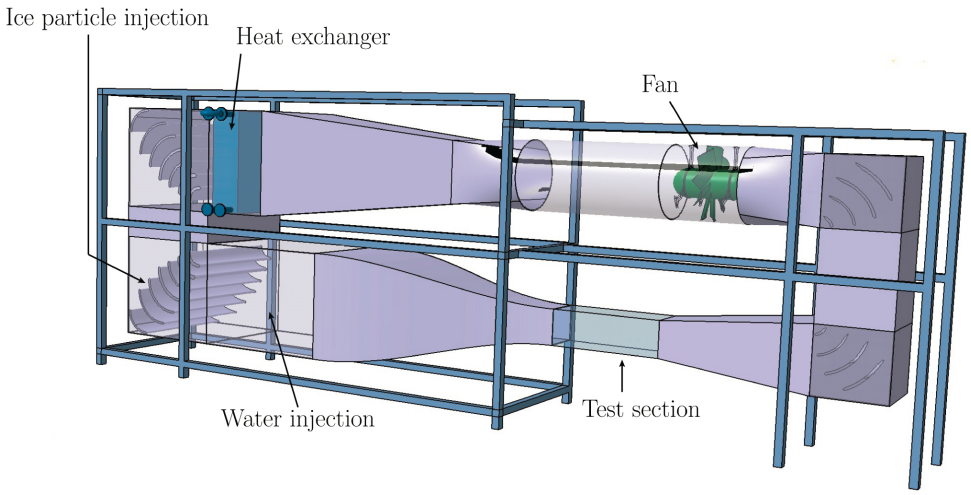

Figure 1. Overview of the wind tunnel

The supply of the water droplets is realized by a water injection system. This water injection system is located directly in front of the nozzle. Five horizontally aligned bars with integrated pneumatic atomizers are mounted at different heights inside the wind tunnel. With the existing spray system a liquid water content between LWC ≈ 1.3 g/m^3 and LWC ≈ 5 g/m^3 depending on the flow velocity is achievable with a uniform distribution inside the test section. The generated droplets have a size between $d_\mathrm{p} = 70$ μm and $d_\mathrm{p} = 95$ μm (MVD).

2.2. Ice particle generation

The ice particles are generated from a humid air flow in a low-temperature balloon and then injected into the wind tunnel. The shapes and size distribution of the produced ice particles are characterized using a high-speed imaging probe. Several different conditions were tested to investigate the influence of the temperature and the transport system of the ice crystals. Most of the captured particles are irregular shaped particles or agglomerates with a mean size between $d_p = 110$ μm and $d_p = 170$ μm.

2.3. Experimental cell

A cylindrical target for studying ice crystal accretion is shown in Fig. 2. The cylinder has an outer diameter of 60 mm, a length of 140 mm and consists of two shells of different materials, thus the cylinder is hollow. The back of the cylinder is made out of polyvinyl chloride (PVC) with a wall thickness of 5 mm to reduce the heat conduction. In contrast the front of the cylinder consists of several layers. The different layers are shown in figure 2.

The first layer (1) in figure 2 is a 0.2 mm thin aluminum sheet which protects the sensors and ensures that there are no disturbances on the surface, which may lead as a starting point for ice growth. The aluminum sheet is made of an AlMn0.5Mg0.5 alloy (EN AW-3105) to prevent corrosion as well as to ensure a high heat conductivity and is attached to the cylinder by a special binding. The binding is a two-component adhesive by Loctite of type EA 9497, which has a high thermal conductivity. It is shown as layer (2) in figure 2 and has a thickness of about 0.3 mm. Considering the thin metal sheet, the thin adhesive layer as well as its good thermal conductivity, the temperature sensors measure nearly the surface temperature. The third layer (3) consists of aluminum of type EN-AW-Al and has a thickness of 4.5 mm to ensure good heat

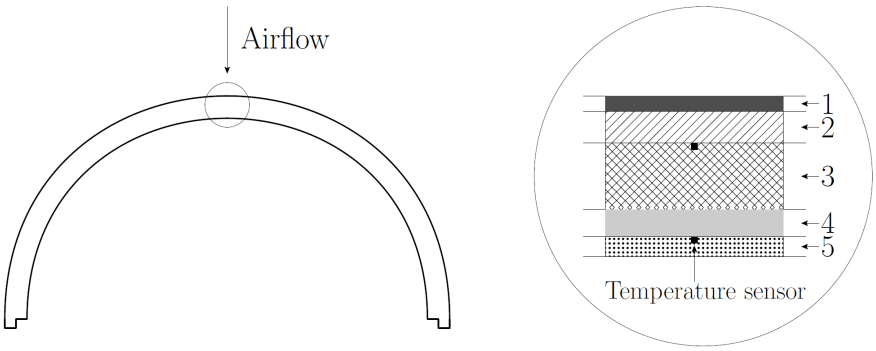

Figure 2. Different layers of the cylinder.

conduction. The temperature sensors are embedded in this layer, which are shown as black squares in figure 2.

On the inside of the cylinder five heating foils (shown as layer (4)) of type KHLV-103/(10)-P are adhered with a pressure sensitive adhesive. Every heating foil is individually controllable and has a power output of $P = 30$ W. This power is distributed over an area of 2.54 cm x 7.62 cm. The heating foils have a thickness of about 0.18 mm. Consequently, a maximum power of $P = 150$ W can be introduced into the shell of the cylinder, which leads to a heat flux of $\dot{q} = 15500.031$ W/m^2.

Due to the fact that the resistance of the heating foil is almost constant and does not depend on the temperature, the power of the heating foil can be controlled directly by the supplied voltage. In this constant voltage circuit the current which flows through the foil is automatically adjusted. The knowledge of the resistance, the current as well as the voltage enables the calculation of the introduced power.

Layer (5) includes additional temperature sensors to measure the heat flux and consists of a heat insulating layer to minimize the loss of heat to the air inside of the cylinder. They are mounted on the heating foils by an adhesive.

For the measurement of the surface temperature the front of the cylinder has five grooves on the surface, where temperature sensors are placed. Thereby the sensors are evenly distributed along a quarter of the circumference of the cylinder. The used temperature sensors are platinum thermisters of type PT1000 with the accuracy class A. These sensors were chosen because of the high accuracy of $\pm(0.15 + 0.002|T|)$ °C, where T is the actual temperature in degree Celsius, in the range of -100 °C to 300 °C.

3. Results and discussion

3.1. Observations of ice accretion

Figure 3 shows different ice layer shapes formed on the cylindrical target. An increase of the ambient temperature to values higher than the melting temperature causes a similar change of the shape because of the increased melting ratio. The resulting shape of the ice is influenced by the flow around the cylinder as well as by the mass flux density and composition of the ice stream. The total mass flux of the ice stream is not perfectly constant during the experiments since it requires some time to reach a steady flow (around 40 seconds). The measured average value of the mass flux density, $\dot{m} = 0.33$ kg/(m^2·s), is the same for all the experiments.

Generally, ice accretion is greater where the shear stress is lower (e.g. at the stagnation point) and less at regions of high shear stress. This shear stress includes the effect of the airflow viscosity and the cumulative effects associated with the inclined impacts of ice crystals. Also,

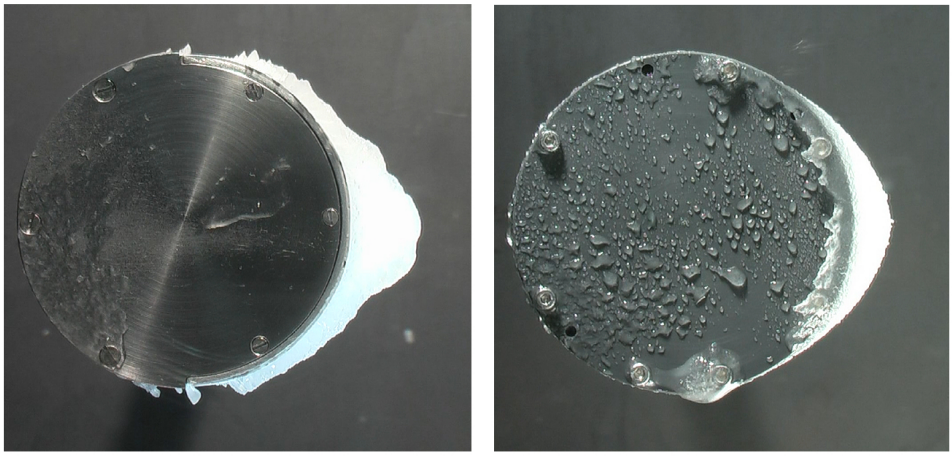

(a) Ice shape for a melting ratio of LWC/TWC = 0.1.

(b) Ice shape for a melting ratio of LWC/TWC = 0.5.

Figure 3. Comparison of the ice shapes for different melting ratios. The average mass flux density, $\dot{m} = 0.33$ kg/(m^2·s), the outer temperature, $T_i = -5$°C, and the exposure time to the ice stream during 120 seconds are the same for both cases.

the collection efficiency is higher at the positions where streamline curvature is high (also at the stagnation point). These two effects are modified as the flow adjusts to the new cylinder shape with accreted ice.

If the amount of water is lower, the accreted ice is harder and less affected by the shear stress. In contrast a high amount of liquid causes the ice to be very soft and deformable. During the experiment the movement of the water on the surface is observable. The water flows over the surface due to flow acting on it. This influences the distribution of water on the surface and the possibility for the ice particle to stick on the surface.

3.2. Evolution of the target temperature: measurements

In Fig. 4 exemplary measurements of the temperature near the cylinder surface at the stagnation point are shown as a function of time for two different cases. In the first case (Fig. 4 left) the cylinder is not heated, its initial temperature is below the freezing point. Impact of a stream of cold dry ice crystals leads to the fast reduction of the temperature. No ice accretion is observed in this case.

In the second case, shown in Fig. 4 (right), the initial temperature of the cylinder is approximately 40°C. The imparting ice particles are melted due to the heat flux which is caused by the positive surface temperature. The specific energy which is needed to melt the ice particles is extracted from the cylinder.

Initially the impacting ice particles are not visible. Only a thin water liquid film is observed on the surface at the early stages. If the surface temperature is decreased ice particles are visible on the surface of the cylinder and move on a liquid layer which is caused by the melting of the particles. As soon as the surface temperature decreases to a value of about 0°C ice starts to accrete on the target surface, beginning at the stagnation point. Based on this first ice accretion more particles then stick to the surface.

3.3. Estimation of the heat transfer coefficient due to ice crystals impacts

Consider the impact of a single dry spherical particle of radius R_0 onto a perfectly rigid substrate. Assume the particle material as semi-brittle, which means a significant plastic deformation before

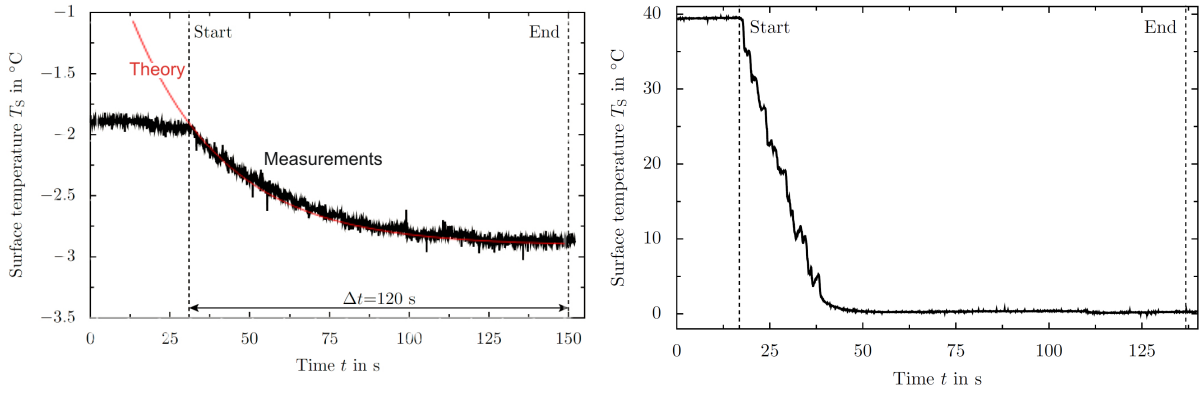

Figure 4. Surface temperature at the stagnation point of the cylinder as a function of time for a non-heated cylinder, in comparison with the theoretical prediction (6) impacted by a dry cold crystals (left graph); and heated cylinder impacted by a mixed stream of liquid drops and ice particles (right graph).

breakup. The stress, appearing at the particle/substrate interface is therefore the yield strength Y_i of ice. The force applied to the particle leads to its deceleration. The equation of motion of an impacting ice crystal particle is solved in [17]. The expressions for the residual maximum impression radius, a_{res}, after collision, the total duration of impact, t_{max} and the total eroded volume of the ice particle are obtained in the form

$$a_{res} \approx R_0 U_0^{1/2} \left(\frac{8\rho_i}{3Y_i}\right)^{1/4}, \quad t_{max} \approx \frac{R_0 \rho_i^{1/2}}{Y_i^{1/2}}, \quad V_{er} \approx \frac{4\pi R_0^3 \rho_i U_0^2}{6Y_i} \tag{1}$$

where U_0 is the ice particle impact velocity, ρ_i is the particle density.

Denote T_i and T_s as the initial uniform temperatures of the ice crystal and the substrate, respectively. The heat flux density during particle contact is determined by the expansion of the thermal boundary layers in the particle and the substrate. While the heat transfer in the substrate is determined by heat conduction, in the particle also convection has to be accounted for, associated with the instantaneous motion of the deforming particle.

The heat transferred from the wall during particle impact can be roughly estimated with the help of (1) as

$$Q_s \approx \int_0^{t_{max}} \pi a_{res}^2 \dot{q} dt = \sqrt{\frac{32\pi}{3}} \frac{4\epsilon_s R_0^{5/2} \rho_i^{3/4} U_0}{Y_i^{3/4}} (T_s - T_{cont}), \tag{2}$$

where ϵ is a thermal effusivity and T_{cont} is a local contact temperature. The heat flux density $\dot{q} = \epsilon_s (T_s - T_{cont})/(\sqrt{\pi t})$ is obtained from the well-known analytical solution for the thermal boundary development as a result of an immediate contact of two solid bodies.

The total heat transferred to the ice particle, Q_i, can be estimated for high speed impacts, if the rate of the particle deformation is higher than the rate of the development of the thermal boundary layer. Consider an adiabatic heating of the eroded volume of the ice particle to the temperature T_{cont} yields the following expression for Q_i:

$$Q_i \approx (T_{cont} - T_i) \rho_i C_{Pi} V_{er}. \tag{3}$$

Equating Q_i and Q_s from (2) and (3) yields the following expression for the total heat transfer associated with a single crystal impact

$$Q_s = A_s (T_s - T_i), \quad A_s = \frac{4\sqrt{6}\epsilon_s \pi R_0^3 \rho_i^2 C_{Pi} U_0^2}{6\sqrt{6}\epsilon_s Y_i - 3\sqrt{\pi} R_0^{1/2} \rho_i^{5/4} C_{Pi} U_0 Y_i^{3/4}}. \tag{4}$$

Next, the heat flux density associated with an impact of a stream of dry ice particles is estimated by

$$\dot{q}_{stream} = Q_s \frac{3\dot{m}}{4\rho_i \pi R_0^3}. \tag{5}$$

Finally, in the absence of phase change on the target surface, the evolution of the substrate temperature T for non-heated target is expressed in the form:

$$T = T_i + \exp\left[-\frac{3\eta A_s \dot{m} t}{4\rho_i \pi R_0^3 c_{Ps} h \rho_s}\right](T_s - T_i), \tag{6}$$

where $\eta = 0.5$ is a correction factor, which takes into account the the fact that expression (2) is an upper bound for Q_s and does not consider the evolution of the impression radius in time.

The theoretical prediction for the surface temperature T is compared with the experimental data in Fig. 4 (left). The agreement between the theory and experiments is rather good. This means that we have developed a theoretical tool which can help to predict the time required for the ice accretion inception.

3.4. Time required for inception of ice crystals accretion

In the case of target heating the evolution of the cylinder surface is expressed in the form

$$T = T_i + \frac{\dot{q}_H}{B_s} + \exp\left[-\frac{B_s t}{\rho_s c_{Ps} h}\right]\left(T_s - T_i - \frac{\dot{q}_H}{B_s}\right), \quad B_s \equiv \frac{3\eta A_s \dot{m}}{4\rho_i \pi R_0^3}. \tag{7}$$

where $\dot{q}_H$ is the heat flux density corresponding to the target heating. An approximate solution for the time required for the ice accretion inception, $t_{accretion}$, is found equating the temperature in (7) to the melting temperature

$$t_{accretion} \approx \frac{\rho_s c_{Ps} h}{B_s}\left|\frac{T_s}{T_i}\right|. \tag{8}$$

Since the initial substrate temperature $T_s \sim \dot{q}_H$, the time of accretion inception should be proportional to the heating power. This conclusion is confirmed by the linear dependence of the inception time on the heating power, shown in Fig. 5 for various liquid-to-total water content ratios.

It should be noted that the scatter of the data, especially for the cases of the mixed liquid/solid water stream, is caused by some difficulties in an exact definition of the instant of accretion inception. In all the cases the inception time is reduced by the presence of the liquid water. This time reduction can be explained increase of the collision time of each single wet particle. Moreover, in some cases, when the viscous and capillary forces associated with the liquid water film are significant, small ice particles can be deposited on the target surface even at positive surface temperatures [19]. These particles can then initiate ice accretion. More accurate analysis of the accretion of mixed ice stream is required, which accounts for the main physical influences. This will be the topic of our future investigations.

4. Conclusions

This paper is focused on the experimental investigation of ice crystal accretion. The time required for the ice accretion inception is measured. It is discovered that accretion is initiated on a heated substrate when its surface temperature is reduced to the melting temperature.

The evolution of the surface temperature is determined by the cooling effects of the impacting cold ice crystals. A theoretical model is developed, which is able to predict the evolution of the target temperature and the instant corresponding to the inception of the ice crystal accretion.

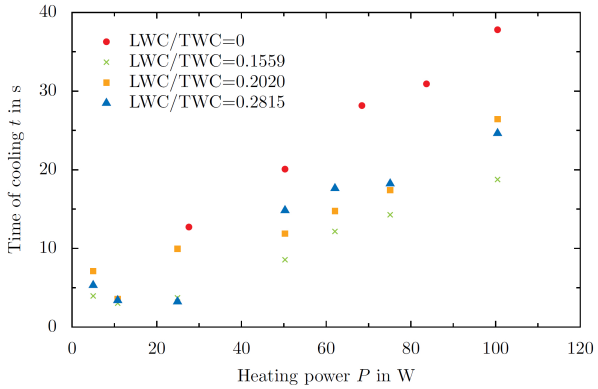

Figure 5. Cooling time of cylinder as a function of the melting ratio of the impacting stream and heating power of the target.

References

[1] Huang J 2009 *Aviation safety through the rule of law* (*Aviation law and policy series* vol 5) (Wolters Kluwer Law & Business)
[2] International Air Transport Association 2015 Safety repost 2014
[3] Mason J, Strapp W and Chow P The ice particle threat to engines in flight
[4] Pruppacher H R and Klett J D 2010 *Microphysics of Clouds and Precipitation* 1st ed (*Atmospheric and Oceanographic Sciences Library* vol 18) (Springer Science+Business Media B.V)
[5] Addy H E 2000 Ice accretions and icing effects for modern airfoils NASA technical paper 210031
[6] Bräunling W J 2009 *Flugzeugtriebwerke* 3rd ed VDI-Buch (Springer-Verlag Berlin Heidelberg)
[7] Federal Aviation Administration 4 November 2014 Airplane and engine certification requirements: Supercooled large drop, mixed phase, and ice crystal icing conditions
[8] Launiainen J and Lyyra M 1986 *Journal of Glaciology* (Vol. 32, No. 110)
[9] Lozowski E P, Stallabrass J R and Hearty P F 1983 *J. Climate Appl. Meteor.* **22**(12) 2053–2062
[10] Lozowski E P, Stallabrass J R and Hearty P F 1983 *J. Climate Appl. Meteor.* **22**(12) 2063–2074
[11] Al-Khalil K, Irani E and Miller D Mixed phase icing simulation and testing at the cox icing wind tunnel
[12] Mason J G, Chow P and Fuleki D M 2011 *J. Eng. Gas Turbines Power* **133**(4) 41201
[13] Struk P, Currie T, Wright W B, Knezevici D C, Fuleki D, Broeren A, Vargas M and Tsao J C 2011 Fundamental ice crystal accretion physics studies *SAE 2011 International Conference on Aircraft and Engine Icing and Ground Deicing* SAE Technical Paper Series (Warrendale, PA, United States)
[14] Currie T C, Struk P M, Tsao J C, Fuleki D and Knezevici D C 2012 Fundamental study of mixed-phase icing with application to ice crystal accretion in aircraft jet engines *4th AIAA Atmospheric and Space Environments Conf., AIAA 2012–3035, New Orleans, LA, 25–28 June*
[15] Currie T C, Fuleki D, Knezevici D C and MacLeod J D 2013 Altitude scaling of ice crystal accretion *5th Atmospheric and Space Environments Conference*
[16] Hauk T, Bonaccurso E, Roisman I V and Tropea C 2015 *Proc. R. Soc. A* **471**(2181) 20150399
[17] Roisman I V and Tropea C 2015 *Proc. R. Soc. A* **471** 20150525
[18] Baumert A, Bansmer S E and Bacher M 2015 Implementation of an innovative ice crystal generation system to the icing wind tunnel braunschweig *53rd AIAA Aerospace Sciences Meeting*
[19] Antonyuk S, Heinrich S, Deen N and Kuipers H 2009 *Particuology* **7** 245–259